

Quantum tricritical point in the temperature-pressure-magnetic field phase diagram of CeTiGe₃Udhara S. Kaluarachchi,^{1,2} Valentin Taufour,^{1,*} Sergey L. Bud'ko,^{1,2} and Paul C. Canfield^{1,2}¹*Ames Laboratory, US Department of Energy, Iowa State University, Ames, Iowa 50011, USA*²*Department of Physics and Astronomy, Iowa State University, Ames, Iowa 50011, USA*

(Received 7 November 2017; revised manuscript received 8 January 2018; published 22 January 2018)

We report the temperature-pressure-magnetic-field phase diagram of the ferromagnetic Kondo-lattice CeTiGe₃ determined by means of electrical resistivity measurements. Measurements up to ~ 5.8 GPa reveal a rich phase diagram with multiple phase transitions. At ambient pressure, CeTiGe₃ orders ferromagnetically at $T_C = 14$ K. Application of pressure suppresses T_C , but a pressure-induced ferromagnetic quantum criticality is avoided by the appearance of two new successive transitions for $p > 4.1$ GPa that are probably antiferromagnetic in nature. These two transitions are suppressed under pressure, with the lower-temperature phase being fully suppressed above 5.3 GPa. The critical pressures for the presumed quantum phase transitions are $p_1 \cong 4.1$ GPa and $p_2 \cong 5.3$ GPa. Above 4.1 GPa, application of magnetic field shows a tricritical point evolving into a wing-structure phase with a quantum tricritical point at 2.8 T at 5.4 GPa, where the first-order antiferromagnetic-ferromagnetic transition changes into the second-order antiferromagnetic-ferromagnetic transition.

DOI: [10.1103/PhysRevB.97.045139](https://doi.org/10.1103/PhysRevB.97.045139)**I. INTRODUCTION**

Quantum phase transitions (QPTs) in metallic ferromagnets have been studied for many years and remain a subject of great current interest [1]. The paramagnetic (PM) to ferromagnetic (FM) transition can be suppressed with nonthermal control parameters such as pressure, chemical composition, and external field, often leading to a $T = 0$ K QPT. However, according to the current theoretical models, when suppressing the FM phase with a clean parameter such as pressure, a continuous PM to FM transition is not possible. Instead, the transition becomes first order, or a modulated magnetic phase can appear. The possibility of a first-order transition or the appearance of modulated magnetic phases was first discussed in Refs. [2,3]. In the case of the transition becoming first order, a wing structure was predicted in Ref. [4] and observed in UGe₂ [5] and ZrZn₂ [6]. The case of the appearance of a modulated magnetic phase is more complex [2,3,7–12], and experimental examples were found in LaCrGe₃ [12] and CeRuPO [13]. Observation of both tricritical wings and modulated magnetic phase in LaCrGe₃ is a good example of a complex phase diagram and provides a different example of the richness of the phase diagram of metallic quantum ferromagnets [14]. Recently, Belitz and Kirkpatrick proposed that such a complex phase diagram is due to quantum fluctuation effects [15].

Cerium-based compounds have attracted attention due to interesting ground states, such as heavy-fermion, unconventional superconductors [16,17], the Kondo insulator [18], magnetic ordering [19,20], etc. Whereas many Ce-based compounds manifest an antiferromagnetic (AFM) ground state, only a few systems are known with FM order and pronounced Kondo effects. CeRuPO [13], CeAgSb₂ [21,22], CeNiSb₃ [23], CePd₂Ge₃ [24], and Ce₂Ni₅C₃ [25] are some examples of the

Ce-based ferromagnets, which show complex phase diagrams under the application of pressure. Interestingly, the FM transition in these materials is suppressed with the pressure, and new magnetic (most likely AFM) phases appear before the Curie temperature reaches 0 K, but no wing structure in the T - H - p phase diagrams has been observed so far. According to the recent theoretical work by Belitz and Kirkpatrick [15], it is possible to have unobservable tricritical wings inside the AFM dome. In most of these cases, the lack of in-field measurements under pressure prevents us from constructing the temperature-pressure-field phase diagram and getting a better understanding of the system. Therefore, it is interesting to further investigate the temperature-pressure-field effect on a Ce-based ferromagnetic system. To address this, we present measurements of electrical resistivity under pressure up to ~ 5.8 GPa and magnetic field up to 9 T on ferromagnetic CeTiGe₃.

CeTiGe₃ is one of the relatively rare examples of a ferromagnetic Kondo lattice ($\gamma = 75$ mJ mol⁻¹ K⁻² [26]); it orders with a Curie temperature $T_C = 14$ K [27]. It crystallizes in the hexagonal perovskite BaNiO₃-type structure ($P6_3/mmc$) [27]. Magnetization measurements show highly anisotropic behavior with the c axis being the easy axis of magnetization [26]. A Curie-Weiss fit to the susceptibility data yields an effective moment of $2.5 \mu_B$, consistent with the reported values [26] and nearly equal to the value for free-ion trivalent Ce ($2.54 \mu_B$). The reported saturation moment at 2 K from the magnetization data ($1.72 \mu_B/\text{Ce}$) along the c axis [26] is comparable with the value obtained from the neutron diffraction study ($1.5 \mu_B/\text{Ce}$) [28]. Substitution of titanium by vanadium (CeTi_{1-x}V_xGe₃) causes a suppression of the Curie temperature down to 3 K at $x = 0.3$ and suggests a possible quantum critical point or phase transition near $x \approx 0.35$ [28]. In contrast to the effect of substitution, a very small, initially positive pressure derivative of T_C ($dT_C/dp \approx 0.3$ K GPa⁻¹ up to 1 GPa) suggests that CeTiGe₃ is located near the maximum of the magnetic ordering temperature in the Doniach model

*Present address: Department of Physics, University of California, Davis, California 95616, USA.

[28]. However, all substitution and pressure measurements have been done on the polycrystalline material and only to modest pressure, $p < 1$ GPa. To get a better understanding of the T - p - H phase diagram, possible FM instability, and quantum critical points it is important to perform high-pressure studies on single-crystalline samples of CeTiGe_3 over a wide pressure range.

II. EXPERIMENTAL METHODS

Single crystals of CeTiGe_3 were grown using a high-temperature solution growth technique [29,30]. A mixture of elemental Ce, Ti, and Ge was placed in a 2-mL fritted alumina crucible [31] with a molar ratio of Ce:Ti:Ge = 4:1:19 [26] and was sealed in a silica ampule under a partial pressure of high-purity argon gas. The sealed ampule was heated to 1200 °C over 10 h and held there for 5 h. It was cooled to 900 °C over 120 h, and excess liquid was decanted using a centrifuge. A good-quality sample (based on the residual resistivity ratio) for the pressure study was selected after ambient-pressure characterization by the magnetization and resistivity measurements. Temperature- and field-dependent resistance measurements were carried out using a Quantum Design Physical Property Measurement System from 1.8 to 300 K. The ac resistivity ($f = 17$ Hz) was measured with the standard four-probe method with the 1-mA current in the ab plane. Four Au wires with diameters of 12.5 μm were spot welded to the sample. A magnetic field, up to 9 T, was applied along the c axis, which corresponds to the magnetization easy axis [26]. A modified Bridgman cell [32] was used to generate pressure for the resistivity measurement. A 1:1 mixture of n -pentane:isopentane was used as a pressure medium. The solidification of this medium occurs around ~ 6 -7 GPa at room temperature [33–37]. The pressure at low temperature was determined by the superconducting transition temperature of Pb [38].

III. RESULTS AND DISCUSSION

The temperature dependencies of the in-plane resistivity of single-crystalline CeTiGe_3 under various pressures up to 5.76 GPa are shown in Fig. 1(a). At ambient pressure, the resistivity exhibits typical Kondo-lattice behavior with a broad minimum of ~ 190 K followed by a maximum at $T_{\text{max}} = 31$ K. T_{max} is assumed to be related to the Kondo interaction with a changing population of crystal electric field levels [26,39–41]. The FM transition manifests itself in the resistivity data as a sharp drop at $T_C = 14.2$ K. Similar values of T_C have been reported from polycrystalline and single-crystalline samples [26–28]. The residual resistivity ratio is 19, a value that suggests a rather good quality of the sample. Upon application of pressure the resistivity at room temperature increases linearly with a rate of $7.4 \mu\Omega \text{ cm GPa}^{-1}$ over the whole pressure range [see the inset of Fig. 1(a)], and both the local maximum and local minimum in the resistivity broaden and move to higher temperatures with increasing pressure. The evolution of the low-temperature resistivity is shown in Fig. 1(b); data are offset by increments of $10 \mu\Omega \text{ cm}$ for clarity.

Figure 2 shows the evolution of the low-temperature resistivity and its temperature derivatives in three selected pressure

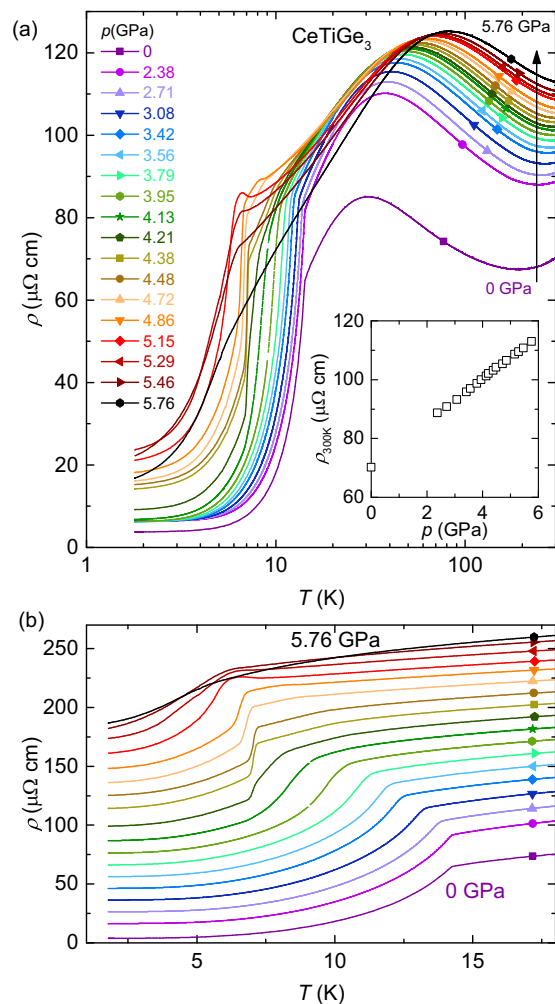


FIG. 1. (a) Temperature dependence of the in-plane resistivity $\rho(T)$ of a CeTiGe_3 single crystal under various pressures p up to 5.76 GPa on a semilog plot. The resistivity at 300 K linearly increases with the pressure at a rate of $7.4 \mu\Omega \text{ cm GPa}^{-1}$ from 0 to 5.76 GPa, as shown in the inset. (b) Low-temperature resistivity at various pressures. Data are offset by increments of $10 \mu\Omega \text{ cm}$ for clarity.

regions; (i) $p < 4.1$ GPa (ii) $4.1 \text{ GPa} < p < 5.3$ GPa, and (iii) $p > 5.3$ GPa. Below 4.1 GPa the FM transition is seen as a sharp change in the slope in the resistivity, and transition temperature is obtained from the sharpest increase of $d\rho/dT$ [black square in Figs. 2(a) and 2(b)]. The FM transition temperature initially shows a weak increase with pressure and then decreases with further applied pressure up to 4.1 GPa. Between 4.1 and 5.3 GPa, the onsets of magnetic transition 1 (MP1) and magnetic transition 2 (MP2) are revealed as a kink/upturn and a sharp drop in the $\rho(T)$, as shown in Figs. 2(c)–2(e). From the transport measurements we cannot unambiguously identify MP1 and MP2 (and MP1', MP3, and MP4) as the magnetic phases. However, observation of the metamagnetic transitions under application of field [see Fig. 5(c) below] strongly suggests that these are probably magnetic phases. The features in the resistivity can be clearly seen in the temperature derivative of the resistivity (right axis of Fig. 2). Transition temperatures of PM-MP1 and MP1-MP2 are obtained from the kink/minimum [green triangle in

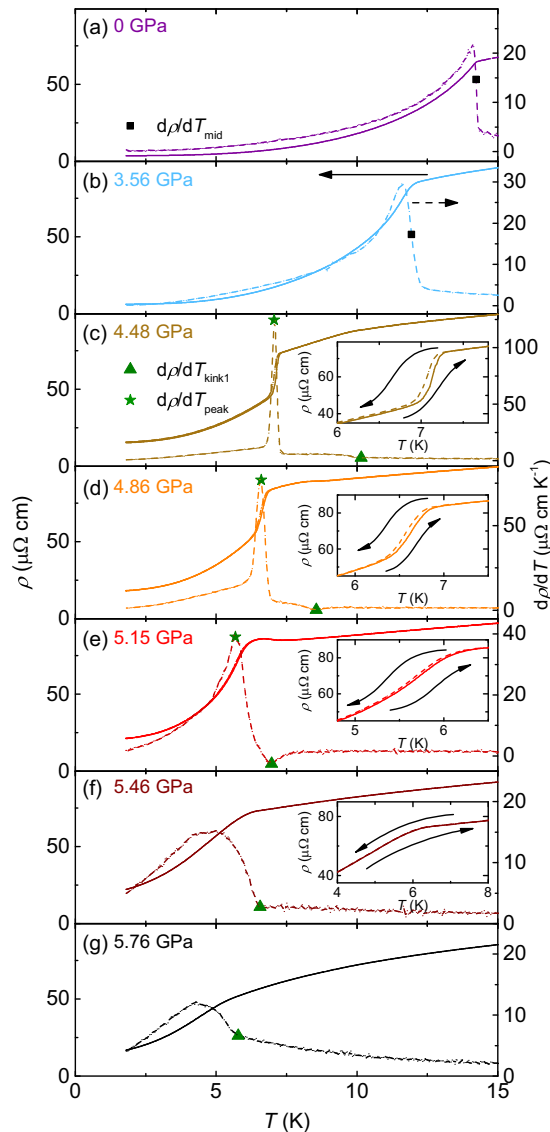


FIG. 2. Low-temperature, in-plane resistivity (left axis) and its corresponding temperature derivative (right axis) of CeTiGe_3 for several representative pressure regions: (a) and (b) $p < 4.1$ GPa, (c)–(e) $4.1 \text{ GPa} < p < 5.3$ GPa, and (f) and (g) $5.3 \text{ GPa} < p$. The solid symbols mark the characteristic temperatures that are associated with phase transitions: black square, PM to FM; green triangle, PM to MP1/MP1'; and green star, MP1 to MP2. The insets of (c)–(e) show the observed hysteretic behavior at their representative pressures. However, no hysteretic behavior is observed above 5.3 GPa, as shown in inset of (f).

Figs. 2(c)–2(e) and sharp peak (green star) in $d\rho/dT$ [Figs. 2(c)–2(e)], respectively. Although the magnetic-ordering wave vector of MP1 is unknown, the feature in the resistivity is similar to that associated with superzone gap formation [42] and suggests an AFM nature for MP1. Both MP1 and MP2 transitions are observed between 4.1 and 5.3 GPa, and thermal hysteresis in ρ for MP2 up to 5.3 GPa [insets of Figs. 2(c)–2(e)] indicates a first-order nature for this transition. On a further increase in pressure, above 5.3 GPa, MP2 disappears, and a new magnetic transition, MP1', continues to decrease with the increase in pressure; no thermal

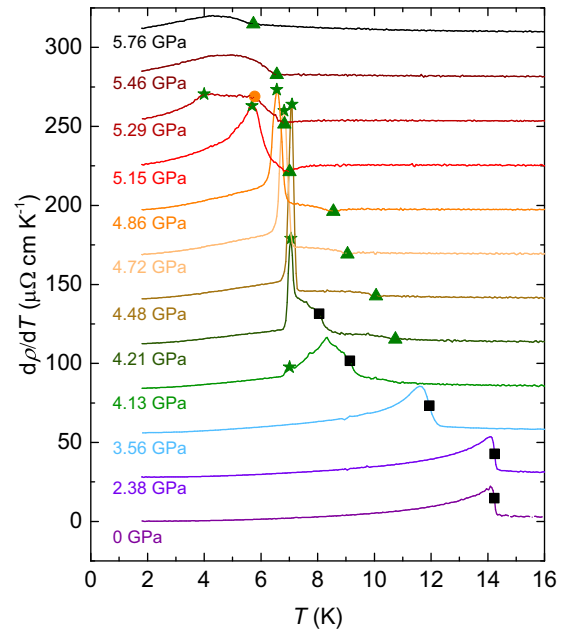


FIG. 3. Evolution of the temperature derivative of the resistivity at low temperature for representative pressures. The data are vertically offset by $28 \mu\Omega \text{ cm K}^{-1}$ to reduce overlap. Solid symbols represent the criteria described in Fig. 2. At 5.29 GPa there is an additional anomaly in $d\rho/dT$, as shown by the orange circle.

hysteresis is observed [Figs. 2(f)–2(g)]. Although features in $\rho(T)$ corresponding to the MP1 and MP1' transitions look similar, it is unclear whether it is the same phase or not. Figure 3 shows the evolution of the temperature derivative of the resistivity for representative pressures. Solid symbols represent the criteria described in Fig. 2.

The temperature-pressure (T - p) phase diagram of CeTiGe_3 obtained from the resistivity measurements is summarized in Fig. 4(a). At low pressures, the Curie temperature of the ambient-pressure, FM phase (solid squares) shows a very weak pressure dependence and then decreases with pressure. For $4.1 \text{ GPa} \leq p \leq 5.3 \text{ GPa}$, there is evidence for two phase transitions, MP1 and MP2, in the $\rho(p, T)$ curves, which interrupt the initial FM phase-transition line. The merging of the PM-FM, PM-MP1, and FM-MP1 transition lines is called the Lifshitz point [43]. The second-order PM-FM transition becomes first order at a tricritical point (TCP; see below), as shown by the horizontal arrow. A similarly complex T - p phase diagram has been observed in CeNiSb_3 [23] and the recently studied itinerant ferromagnet LaCrGe_3 [12]. Pressure-induced transitions from the FM to AFM state are also observed in several other Ce-based compounds, such as CeAgSb_2 [22], CeNiSb_3 [23], CePd_2Ge_3 [24], $\text{Ce}_2\text{Ni}_5\text{C}_3$ [25], and CeRuPO [13]. Above 5.3 GPa, the low-temperature MP2 phase disappears, and MP1' continues to decrease with the increase in pressure. As mentioned above, it is unclear whether there is a phase boundary between MP1 and MP1' near 5.3 GPa.

In addition to the T - p phase diagram, we find that T_{max} exponentially increases from 31 to 82 K upon increasing pressure [Fig. 4(b)]. The smooth change in T_{max} indicates that the existence of the new phases is not associated with a discontinuous change in the electronic or crystal structure or

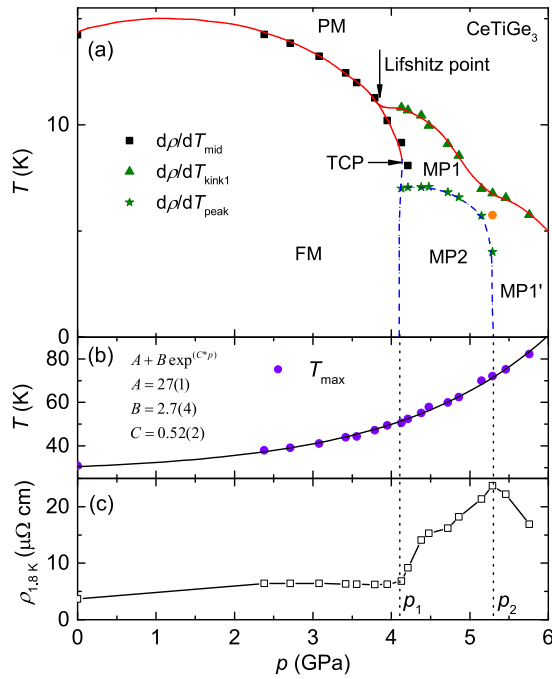


FIG. 4. (a) T - p phase diagram of CeTiGe_3 in zero applied field. Transition temperatures are determined from the anomalies in $d\rho/dT$, as shown in Figs. 2 and 3. The values of critical pressure p_1 and p_2 are 4.1 and 5.3 GPa, respectively. Solid lines are a guide to the eye, and dashed lines are suggested extrapolations of phase boundaries. The red and blue lines represent the second- and first-order phase transitions. The vertical and horizontal arrows represent the Lifshitz and tricritical points, respectively. (b) Maximum in resistivity T_{max} [shown in Fig. 1(a)] as a function of pressure increase as an exponential function. (c) Pressure dependence of ρ at 1.8 K.

crystal electric field splitting. Figure 4(c) shows the pressure evolution of the resistivity at 1.8 K. The results show breaks in $\rho_{1.8\text{K}}(p)$ at p_1 (FM to MP2) and a maximum at p_2 (MP2 to MP1). The exact nature of the phase transitions at p_1 and p_2 is not known, and to resolve this, it would be useful to study the magnetic-ordering wave vector under pressure.

Application of an external magnetic field adds another dimension to our phase diagram, and different behavior of the resistivity anomalies under magnetic field allows us to explore further new phase regions of this material. Figure 5(a) shows the temperature dependence of ρ at different magnetic fields, applied along the c axis, at 4.48 GPa. The sharp drop in the resistivity at low fields ($\mu_0 H \leq 0.3$ T) broadens at higher fields. These data manifest hysteretic behavior up to 0.5 T, indicating the first-order nature of the transition. The zero-field kink in the resistivity, at 9.8 K, changes into a hump with the increase in field (0.25 T) and disappears at 0.3 T. Another humplike feature appears above 0.35 T and broadens with a further increase in the field. These features can be clearly observed in the temperature derivative shown in Fig. 5(b).

The field dependence of ρ ($p = 4.48$ GPa) below 7 K shows a metamagnetic transition with a low-field plateau followed by a steplike feature and develops into two transitions above 7 K [Fig. 5(c)]. The solid and dashed lines represent the field increasing $\rho_{\text{up}}(H)$ and decreasing $\rho_{\text{down}}(H)$, respectively. The difference between $\rho_{\text{up}}(H)$ and $\rho_{\text{down}}(H)$ shows a sizable

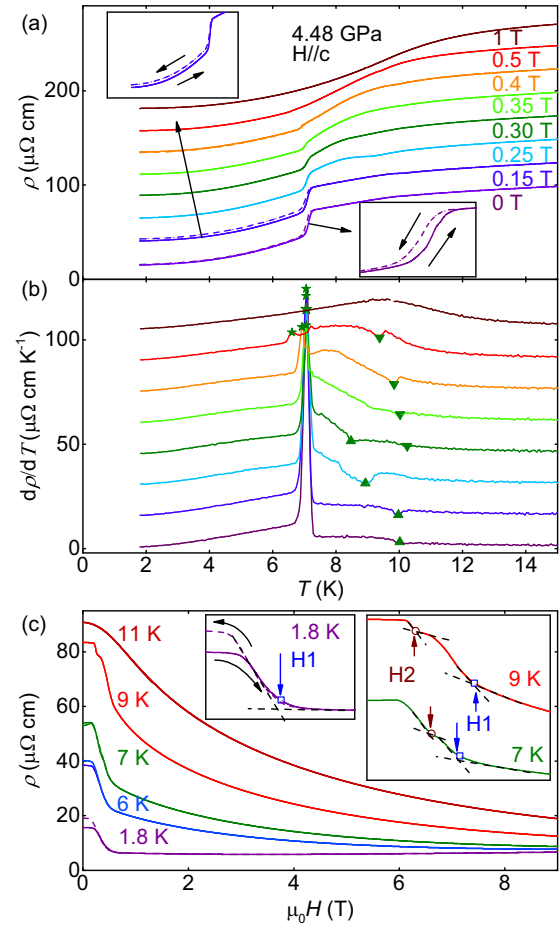


FIG. 5. (a) Temperature dependence of the resistivity at various fixed fields for $p = 4.48$ GPa and $H \parallel c$. The data are vertically shifted by an integer of $25 \mu\Omega \text{ cm}$ to avoid overlapping. The insets show the observed hysteretic behavior in the temperature scan. Solid and dashed lines represent the temperature increasing and decreasing, respectively. (b) Corresponding temperature derivative $d\rho/dT$ of (a). The data are vertically shifted by an integer of $15 \mu\Omega \text{ cm K}^{-1}$ to avoid overlapping. Solid symbols represent the criteria used to obtain the transition temperatures at various magnetic fields. (c) Field dependence of the resistivity at fixed temperatures. For these data the sample was cooled in zero field, and then $\rho(H)$ data were collected for increasing field ρ_{up} and then decreasing field ρ_{down} . Then the temperature was increased to the desired value, and data were collected for increasing and decreasing field. Solid and dashed lines represent the field increasing and decreasing, respectively. Insets show the observed hysteretic behavior and the criteria used to obtain the transition fields. Above 7 K no hysteretic behavior is observed.

deviation (ρ is smaller in the increasing field than in the decreasing field) for the $0 \leq H \leq 0.3$ T range. In Fig. 5, hysteresis is apparent not only in the transition temperature [Fig. 5(a)] and transition field [Fig. 5(c)] but also in the magnitude of the resistivity. Similar hysteretic behavior is observed in CeAuSb_2 [44–46] and $\text{CeTAl}_4\text{Si}_2$ ($T = \text{Rh, Ir}$) [47]. Based on the hysteretic behavior, we can conclude these metamagnetic transitions are likely associated with a first-order phase transition. The observed hysteresis in the magnitude of resistivity indicates the possibility of magnetic domains. At temperatures above 11 K, the resistivity shows a very broad

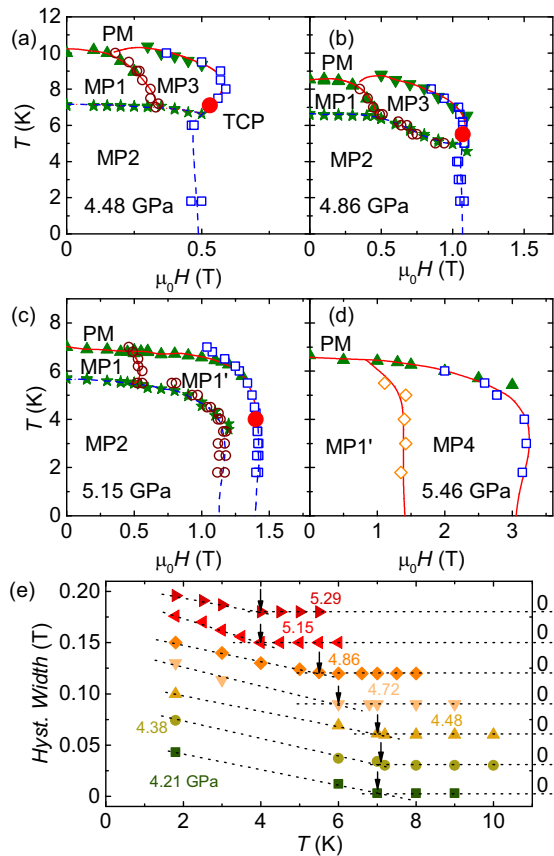


FIG. 6. T - H phase diagrams for various pressures, (a) 4.48, (b) 4.86, (c) 5.15, and (d) 5.46 GPa, determined by tracking various anomalies in temperature and field derivatives of the resistivity measurement as shown in Fig. 5. Solid and open symbols represent transition temperatures determined by T sweeps and transition fields determined by H sweeps (as described in Fig. 5), respectively. Dashed blue and solid red lines indicate the first-order and second-order transitions, respectively. (e) Temperature dependence of hysteresis widths for the transition at H1 at various pressures. The data are vertically offset by 0.03 T to avoid overlap. Vertical arrows represent the estimated tricritical points for each pressure. Zero for each data set is shown on the right-hand axis.

anomaly, and no transition has been observed. Criteria used to obtain transition fields are shown in the inset of Fig. 5(c).

Figures 6(a)–6(d) show the T - H phase diagrams at representative pressures. Transition temperatures determined by T -sweep measurements are shown by solid symbols, and anomalies appearing in isothermal H -sweep measurements are shown by open symbols. Dashed blue and solid red lines indicate the first-order and second-order transitions, respectively (based on the presence or lack of hysteretic behavior respectively). The red circle represents the TCP determined by Fig. 6(e). Temperature dependence hysteresis widths for the transition at H1 are shown in Fig. 6(e). The data are vertically offset by 0.03 T to avoid overlap. Clear hysteresis at low temperature gradually decreases with increasing temperature and disappears at a TCP, as shown by a vertical arrow. In contrast to the wing critical point (WCP) in UGe_2 [5] and LaCrGe_3 [14], here we observed a TCP in the T - H phase diagram where first-order transition changes into the second-order transition. This TCP

corresponds to the boundary of a wing structure similar to that of UGe_2 [5] and LaCrGe_3 [14]. The T - H phase diagrams of CeTiGe_3 for pressures between 4.1 and 5.3 GPa show complex behavior. Three magnetic phases (MP1, MP1', and MP2) are identified by the anomalies in the resistivity measurement. Both MP1 and MP1' phases are separated from the MP2 phase by a first-order transition, as shown in Figs. 6(a)–6(c). For pressures between 4.1 and 5.3 GPa, these T - H phase diagrams are similar to those found for $\text{CeRu}_2\text{Al}_2\text{B}$ [48], which undergoes a second-order AFM transition that is followed by a first-order FM transition as a function of temperature. Above 5.3 GPa, only two magnetic phases, MP1' and MP4, are identified by the resistivity measurements, and there is no longer a first-order phase-transition boundary observed.

Figure 7 shows the constructed T - H phase diagrams for pressures between 4.21 and 5.76 GPa. There is a clear difference in the T - H phase diagrams below 4.86 and above 5.46 GPa. The T - H phase diagram for the intermediate pressure, 5.29 GPa, shows a complex behavior. Also, we observed an additional shoulder like anomaly in $\rho(H)$ at 5.76 GPa [gray stars in Figs. 8(c) and 7]. When the temperature was increased, it became broadened and merged with H1 and was no longer resolvable. H1, H2, and H3 are the anomalies observed in $\rho(H)$ data, as shown in Figs. 5(c), 8(b), and 8(c).

Figure 8(a) shows the field dependence of the resistivity at 1.8 K, $\rho(H)$, for different pressures. For the pressures in between p_1 and p_2 , $\rho(H)$ for an increasing magnetic field shows a clear metamagnetic transition with a substantial (>40%) drop in resistivity. For higher pressures, the sharp drop in $\rho(H)$ disappears, and several metamagnetic transitions can be observed. Figures 8(b) and 8(c) show the representative magnetoresistance data for $4.1 \text{ GPa} < p < 5.3 \text{ GPa}$ and $p > 5.3 \text{ GPa}$, respectively. Transition fields determined by H -sweep measurements are shown by the open symbols. To estimate the transition width, we used the field derivative of the resistivity at 1.8 K, as shown in Figs. 8(d) and 8(e). The minimum at H1 is fitted with Gaussian+linear-background curves and obtained the width of the Gaussian distribution. The blue lines in Figs. 8(d) and 8(e) represent the fitted curves to the data. We noticed that the transition width [Fig. 8(f), right axis] at H1 at 1.8 K remains small for the first-order transition and becomes broad in the second-order regime. Using linear extrapolation as represented by red dashed lines, we obtained pressure corresponding to the TCP at 1.8 K, which is 5.3 GPa. In addition to that, the temperature dependence hysteresis width for transition H1 at 1.8 K is also suppressed with the pressure and disappeared above 5.3 GPa, as shown in Fig. 8(f) (left axis). Figure 8(g) shows the H - p phase diagram at 1.8 K constructed from the above criteria. The magnetic field that corresponds to the H1 transition is shifted up with pressure. Its extrapolation down to zero yields $p \cong 4.1 \text{ GPa}$, which is in agreement with the p_1 obtained from the T - p diagram [Fig. 4(a)]. We observe the increasing rate of metamagnetic transition field with respect to pressure changes near 5.3 GPa.

Similar H - p phase diagrams at low temperature have been observed in LaCrGe_3 [14] and the $\text{CeRu}_2(\text{Si}_{1-x}\text{Ge}_x)_2$ [49,50] system. CeRu_2Ge_2 is a local moment system [51], while CeRu_2Si_2 is itinerant [52]. Application of pressure to CeRu_2Ge_2 gives nearly the same magnetic phase diagram as that of $\text{CeRu}_2(\text{Si}_{1-x}\text{Ge}_x)_2$ [53,54]. Observed transport and

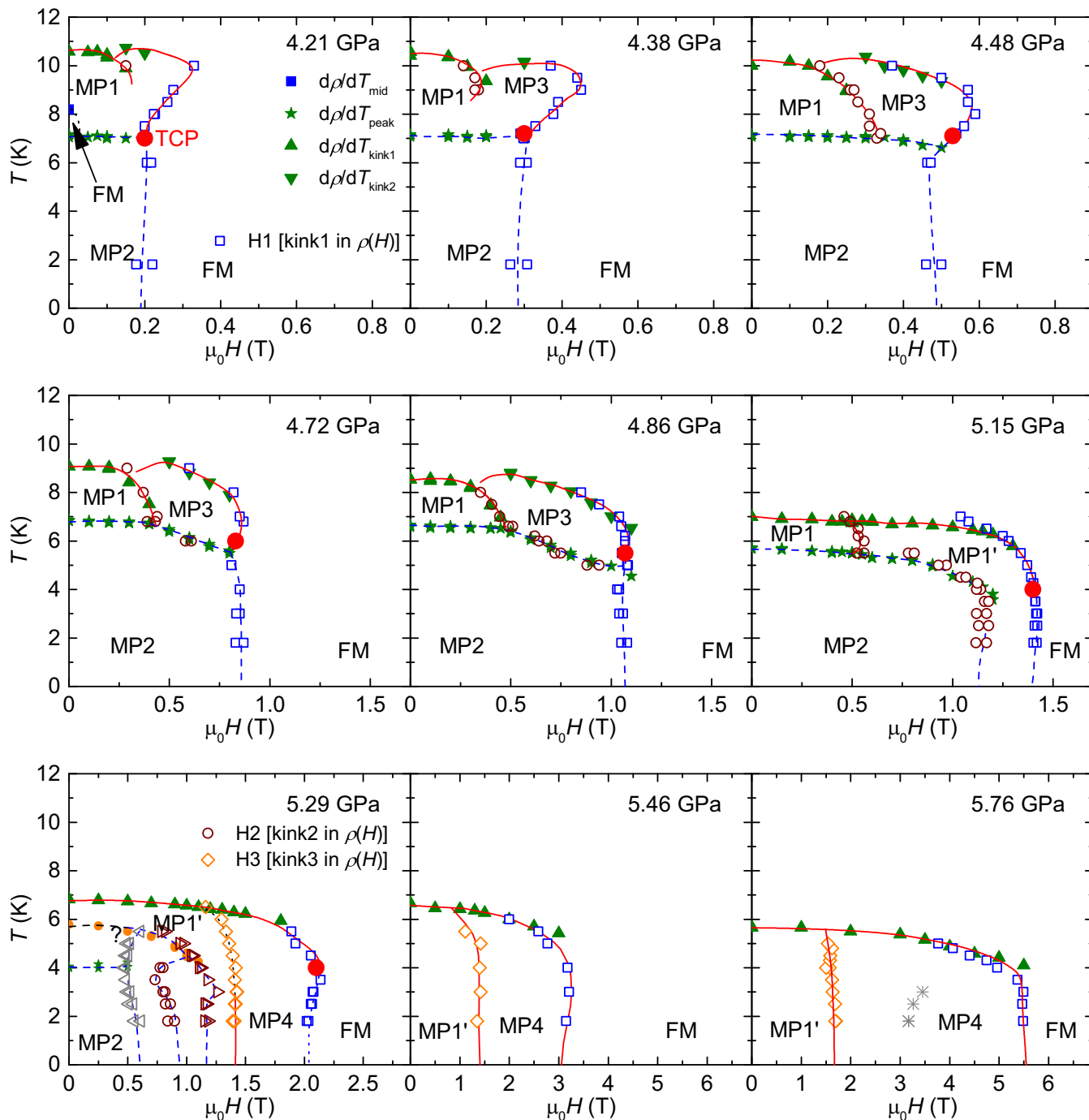


FIG. 7. T - H phase diagrams, including those shown in Figs. 6(a)–6(d), at various increasing applied pressures. At 5.29 GPa, T - H phase diagrams show a complex behavior with additional metamagnetic transitions (gray and brown open triangles) in $\rho(H)$ data (raw data are not shown). H1, H2, and H3 are the anomalies observed in $\rho(H)$ data as shown in Figs. 5(c), 8(b), and 8(c).

de Haas–van Alphen data suggest that, for this system, a change in the f -electron nature from local to itinerant occurs when the FM phase disappears [49]. On the other hand, the itinerant ferromagnet LaCrGe₃ shows tricritical wings as well as modulated magnetic phase. Interestingly, the T - p - H phase diagrams of both LaCrGe₃ [14] and CeRu₂Ge₂ [50] without AFM states are similar to the itinerant weak ferromagnet like UGe₂ [5]. This similarity might imply that the physics behind these phase diagrams are not very different. In UCoAl [55]

an additional anomaly is observed at the end of the tricritical wings similar to what we observe in CeTiGe₃. It is possible that the quantum wing critical point in UCoAl is, in fact, a quantum tricritical point similar to CeTiGe₃. However, the situation is not as clear since, unlike CeTiGe₃, the new anomaly is not observed as a phase boundary in the low-pressure region (i.e., there is no observed Lifshitz point in UCoAl). In addition, the position of the quantum wing critical point in UCoAl is unclear and was proposed to be located at higher pressures [56]. In light

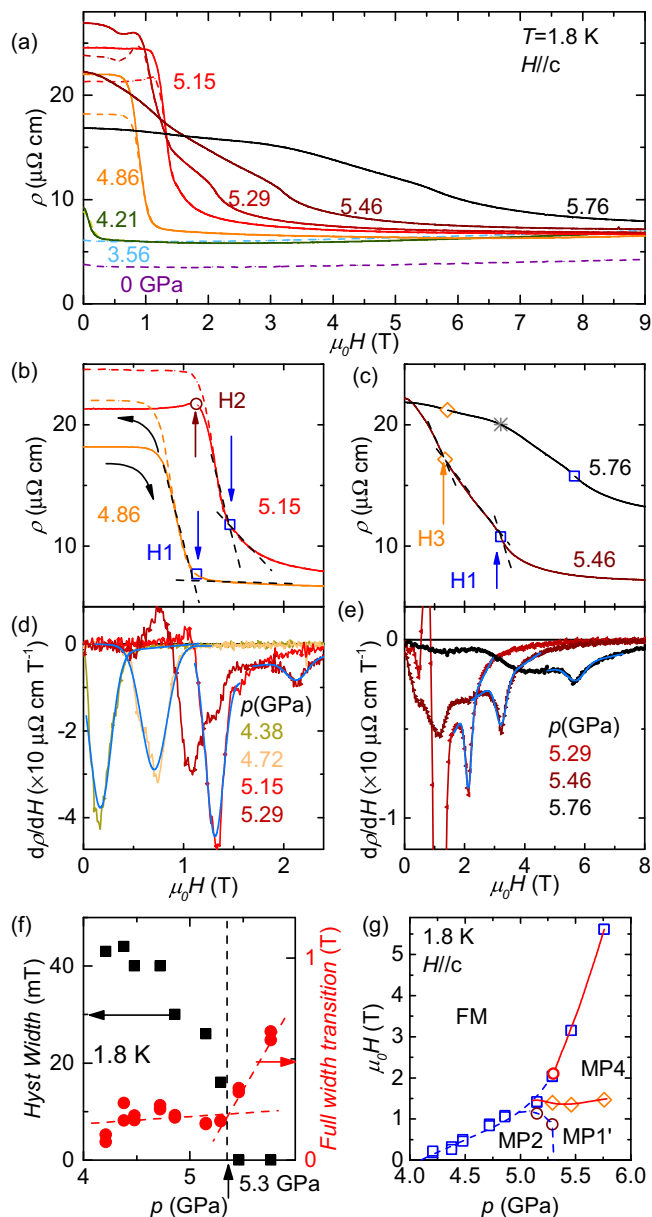


FIG. 8. (a) Field dependence of ρ at 1.8 K for various pressures. Solid and dashed lines represent the field increasing and decreasing, respectively. Representative $\rho(H)$ data for (b) $4.1 \text{ GPa} < p < 5.3 \text{ GPa}$ and (c) $p > 5.3 \text{ GPa}$ and the criteria used to obtain the transition fields at 1.8 K. The open symbols represent the corresponding transition fields. The gray star represents the shoulderlike anomaly that appeared at 5.76 GPa (Fig. 7). (d) and (e) Representative derivative $d\rho/dH$ data for the H1 transition at 1.8 K. The blue lines represent the Gaussian+linear-background fitted curves which are used to obtain the full width of the H1 transition. (f) The left axis shows the pressure dependence hysteresis width of transition H1 at 1.8 K. The right axis shows the pressure dependence of the full width of H1 obtained with $d\rho/dH$ [(d) and (e)] at 1.8 K. The vertical dashed line represents the tricritical pressure $\sim 5.3 \text{ GPa}$ at 1.8 K. (g) H - p phase diagram at 1.8 K based on the criterion shown in (b) and (c). Blue dashed and red solid lines represent the first- and second-order transitions. Red open circle represents the extrapolated QTCP.

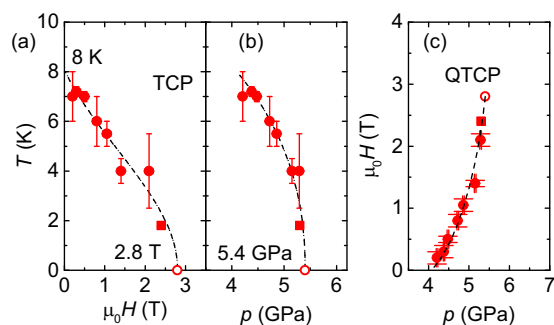


FIG. 9. Projection of the tricritical points (TCPs) in the (a) T - H , (b) T - p , and (c) H - p planes. Red solid circles represent the TCP determined by Fig. 6(e). Red solid squares were obtained from Fig. 8 (f). Dashed lines are guides to the eyes, and open red circles represent the extrapolated QTCP.

of the double-wing structure observed in LaCrGe_3 [14], UGe_2 [57], and ZrZn_2 [58,59], it is also possible that the additional anomaly corresponds to a second wing.

The projections of the tricritical points in the T - H , T - p , and H - p planes are shown in Figs. 9(a), 9(b) and 9(c), respectively. The wing lines can be extrapolated to a quantum tricritical point (QTCP) at 0 K, which is found to be at 2.8 T at 5.4 GPa. The shape of the wings at low temperatures was first reported in Ref. [60] based on the third law of thermodynamics and the Clapeyron-Clausius relations. It was pointed out that the wings are perpendicular to the $T = 0 \text{ K}$ plane but not perpendicular to the p axis [60]. Later on, theoretical analysis based on Landau expansion showed that the slopes of the wings dT/dH and dp/dH are infinite near $H = 0 \text{ T}$ [61]. This was observed experimentally in URhGe [62]. It was also observed in LaCrGe_3 , despite the existence of another magnetic phase [14]. Here we do not observe such behavior ($dT/dH|_{TCP} \rightarrow \infty$) in wings near the TCP, which could be due to the existence of magnetic phase MP1 or to the lack of data near p_1 . More careful measurements near p_1 are required. Also, the TCP at $H = 0 \text{ T}$ is found to be $\sim 8 \text{ K}$, and this is below the MP1 transition. A similar observation was made in LaCrGe_3 [14], where the TCP seems to be located below the Lifshitz point. Recent theoretical description by Belitz and Kirkpatrick [15] shows the complex behavior of the phase diagrams of metallic magnets when an AFM order is observed in addition to the FM phase due to the quantum fluctuations. We observed a QTCP where the first-order AFM-FM transition changes into the second-order AFM-FM transition at 2.8 T at 5.4 GPa [see Fig. 8(g)], similar to what is shown in Fig. 3(a) in Ref. [15]. Very recently, QTCP was experimentally observed in NbFe_2 [63].

The constructed, partial T - p - H phase diagram of CeTiGe_3 based on resistivity measurements is shown in Fig. 10. A FM quantum critical point in CeTiGe_3 is avoided by the appearance of MP1 and MP2 phases and shows a field-induced wing structure above 4.1 GPa. The estimated QTCP is shown by the open red circle. In order to provide a clear picture of the wing-structure phase diagram, we show only selected phases here (see Fig. 7 for H - T phase diagrams at various pressures). In the

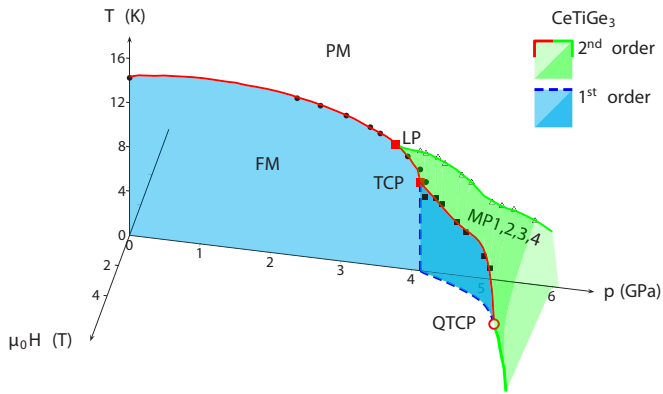


FIG. 10. The constructed, partial T - p - H phase diagram of CeTiGe_3 based on resistivity measurements. Blue surfaces represent the first-order planes, and the green surface represents the second-order $\text{MPI}_{1,2,3,4}$ phase boundary. Solid red and dashed blue lines represent the second- and first-order transitions, respectively. The open circle represents the extrapolated QTCP.

case of the itinerant ferromagnet LaCrGe_3 [12,14], the second-order FM transition becomes first order at a tricritical point in the T - p plane, and application of a magnetic field reveals a wing-structure phase diagram. Appearances of modulated magnetic phase in LaCrGe_3 [14] makes it the first example of a different type of phase diagram of metallic ferromagnets. Unlike LaCrGe_3 (Fig. 5 in Ref. [14]), where wings are extended beyond the AFM phases, the observed wings in CeTiGe_3 are always bounded by the AFM phases. This can be clearly visualized in Fig. 8(g) (for comparison see Fig. 4 in Ref. [14]). The observation of QTCP in metallic magnets in the case of the appearance of AFM order in addition to the FM order is theoretically described by Belitz and Kirkpatrick [15]. This theoretical finding is consistent with our experimental observation of a QTCP in CeTiGe_3 . Therefore, CeTiGe_3 is a good example of a Ce-based compound in which the system can be driven into various magnetic ground

states by fine tuning of the exchange interaction achieved by temperature, pressure, and magnetic field.

IV. CONCLUSIONS

We have measured the high-pressure electrical resistivity of CeTiGe_3 up to 5.8 GPa and 9 T and found a complex T - p - H phase diagram. The ferromagnetic transition at ambient pressure initially slightly increases and then decreases, indicating that CeTiGe_3 is located just below the maximum (left side) of the Doniach phase diagram. The ferromagnetic transition is suppressed near 4.1 GPa, and a cascade of phase transitions is observed above that. The change in residual resistivity near 4.1 and 5.3 GPa suggests a modification of the electronic structure upon entering these magnetic phases. Thus, CeTiGe_3 is another clear example of an avoided ferromagnetic quantum critical point due to the appearance of magnetic phase (probably antiferromagnetic). Application of magnetic field under pressure above 4.1 GPa reveals a wing-structure phase diagram. In contrast to the wing critical point in LaCrGe_3 , we observed a tricritical point in the H - p plane, which corresponds to the boundary of the wing structure. The estimated quantum tricritical point of CeTiGe_3 is located at 2.8 T at 5.4 GPa. We believe that the present work will stimulate further experiments to investigate the properties of this material.

ACKNOWLEDGMENTS

We would like to thank T. Kong, S. Manni, and A. Kreyssig for useful discussions. This work was supported by the US Department of Energy (DOE), Office of Science, Basic Energy Sciences, Materials Science and Engineering Division. The research was performed at Ames Laboratory, which is operated for the US DOE by Iowa State University under Contract No. DE-AC02-07CH11358. V.T. was partially supported by the Critical Material Institute, an Energy Innovation Hub funded by US DOE, Office of Energy Efficiency and Renewal Energy, Advanced Manufacturing Office.

- [1] M. Brando, D. Belitz, F. M. Grosche, and T. R. Kirkpatrick, *Rev. Mod. Phys.* **88**, 025006 (2016).
- [2] D. Belitz, T. R. Kirkpatrick, and T. Vojta, *Phys. Rev. B* **55**, 9452 (1997).
- [3] D. Belitz, T. R. Kirkpatrick, and T. Vojta, *Phys. Rev. Lett.* **82**, 4707 (1999).
- [4] D. Belitz, T. R. Kirkpatrick, and J. Rollbühler, *Phys. Rev. Lett.* **94**, 247205 (2005).
- [5] V. Taufour, D. Aoki, G. Knebel, and J. Flouquet, *Phys. Rev. Lett.* **105**, 217201 (2010).
- [6] N. Kabeya, H. Maekawa, K. Deguchi, N. Kimura, H. Aoki, and N. K. Sato, *J. Phys. Soc. Jpn.* **81**, 073706 (2012).
- [7] A. V. Chubukov, C. Pépin, and J. Rech, *Phys. Rev. Lett.* **92**, 147003 (2004).
- [8] G. J. Conduit, A. G. Green, and B. D. Simons, *Phys. Rev. Lett.* **103**, 207201 (2009).
- [9] U. Karahasanovic, F. Krüger, and A. G. Green, *Phys. Rev. B* **85**, 165111 (2012).
- [10] S. J. Thomson, F. Krüger, and A. G. Green, *Phys. Rev. B* **87**, 224203 (2013).
- [11] C. J. Pedder, F. Krüger, and A. G. Green, *Phys. Rev. B* **88**, 165109 (2013).
- [12] V. Taufour, U. S. Kaluarachchi, R. Khasanov, M. C. Nguyen, Z. Guguchia, P. K. Biswas, P. Bonfà, R. De Renzi, X. Lin, S. K. Kim, E. D. Mun, H. Kim, Y. Furukawa, C.-Z. Wang, K.-M. Ho, S. L. Bud'ko, and P. C. Canfield, *Phys. Rev. Lett.* **117**, 037207 (2016).
- [13] H. Kotegawa, T. Toyama, S. Kitagawa, H. Tou, R. Yamauchi, E. Matsuoka, and H. Sugawara, *J. Phys. Soc. Jpn.* **82**, 123711 (2013).
- [14] U. S. Kaluarachchi, S. L. Bud'ko, P. C. Canfield, and V. Taufour, *Nat. Commun.* **8**, 546 (2017).
- [15] D. Belitz and T. R. Kirkpatrick, *Phys. Rev. Lett.* **119**, 267202 (2017).
- [16] F. Grosche, S. Julian, N. Mathur, and G. Lonzarich, *Phys. B (Amsterdam, Neth.)* **223**, 50 (1996).

- [17] N. D. Mathur, F. M. Grosche, S. R. Julian, I. R. Walker, D. M. Freye, R. K. W. Haselwimmer, and G. G. Lonzarich, *Nature (London)* **394**, 39 (1998).
- [18] M. F. Hundley, P. C. Canfield, J. D. Thompson, Z. Fisk, and J. M. Lawrence, *Phys. Rev. B* **42**, 6842 (1990).
- [19] J. R. Iglesias, C. Lacroix, and B. Coqblin, *Phys. Rev. B* **56**, 11820 (1997).
- [20] S. Evans, A. Bhattacharjee, and B. Coqblin, *Phys. B (Amsterdam, Neth.)* **171**, 293 (1991).
- [21] K. Myers, S. Bud'ko, I. Fisher, Z. Islam, H. Kleinke, A. Lacerda, and P. Canfield, *J. Magn. Magn. Mater* **205**, 27 (1999).
- [22] V. A. Sidorov, E. D. Bauer, N. A. Frederick, J. R. Jeffries, S. Nakatsuji, N. O. Moreno, J. D. Thompson, M. B. Maple, and Z. Fisk, *Phys. Rev. B* **67**, 224419 (2003).
- [23] V. A. Sidorov, E. D. Bauer, H. Lee, S. Nakatsuji, J. D. Thompson, and Z. Fisk, *Phys. Rev. B* **71**, 094422 (2005).
- [24] T. Burghardt, E. Hallmann, and A. Eichler, *Phys. B (Amsterdam, Neth.)* **230**, 214 (1997).
- [25] A. Yamada, K. Matsubayashi, Y. Uwatoko, K. Kondo, S. Katano, and M. Kosaka, *Solid State Commun.* **150**, 725 (2010).
- [26] M. Inamdar, A. Thamizhavel, and S. K. Dhar, *J. Phys.: Condens. Matter* **26**, 326003 (2014).
- [27] P. Manfrinetti, S. Dhar, R. Kulkarni, and A. Morozkin, *Solid State Commun.* **135**, 444 (2005).
- [28] W. Kittler, V. Fritsch, F. Weber, G. Fischer, D. Lamago, G. André, and H. v. Löhneysen, *Phys. Rev. B* **88**, 165123 (2013).
- [29] P. C. Canfield and Z. Fisk, *Philos. Mag. B* **65**, 1117 (1992).
- [30] P. C. Canfield and I. R. Fisher, *J. Cryst. Growth* **225**, 155 (2001).
- [31] P. C. Canfield, T. Kong, U. S. Kaluarachchi, and N. H. Jo, *Philos. Mag.* **96**, 84 (2016).
- [32] E. Colombier and D. Braithwaite, *Rev. Sci. Instrum.* **78**, 093903 (2007).
- [33] N. Tateiwa and Y. Haga, *Rev. Sci. Instrum.* **80**, 123901 (2009).
- [34] G. J. Piermarini, S. Block, and J. Barnett, *J. Appl. Phys.* **44**, 5377 (1973).
- [35] S. Klotz, J.-C. Chervin, P. Munsch, and G. L. Marchand, *J. Phys. D* **42**, 075413 (2009).
- [36] S. K. Kim, M. S. Torikachvili, E. Colombier, A. Thaler, S. L. Bud'ko, and P. C. Canfield, *Phys. Rev. B* **84**, 134525 (2011).
- [37] M. S. Torikachvili, S. K. Kim, E. Colombier, S. L. Bud'ko, and P. C. Canfield, *Rev. Sci. Instrum.* **86**, 123904 (2015).
- [38] B. Bireckoven and J. Wittig, *J. Phys. E* **21**, 841 (1988).
- [39] B. Cornut and B. Coqblin, *Phys. Rev. B* **5**, 4541 (1972).
- [40] K. Hanzawa, K. Yamada, and K. Yosida, *J. Magn. Magn. Mater.* **47**, 357 (1985).
- [41] V. Taufour, H. Hodovanets, S. K. Kim, S. L. Bud'ko, and P. C. Canfield, *Phys. Rev. B* **88**, 195114 (2013).
- [42] A. R. Mackintosh, *Phys. Rev. Lett.* **9**, 90 (1962).
- [43] R. M. Hornreich, M. Luban, and S. Shtrikman, *Phys. Rev. Lett.* **35**, 1678 (1975).
- [44] L. Balicas, S. Nakatsuji, H. Lee, P. Schlottmann, T. P. Murphy, and Z. Fisk, *Phys. Rev. B* **72**, 064422 (2005).
- [45] K.-A. Lorenzer, A. M. Strydom, A. Thamizhavel, and S. Paschen, *Phys. Status Solidi B* **250**, 464 (2013).
- [46] L. Zhao, E. A. Yelland, J. A. N. Bruin, I. Sheikin, P. C. Canfield, V. Fritsch, H. Sakai, A. P. Mackenzie, and C. W. Hicks, *Phys. Rev. B* **93**, 195124 (2016).
- [47] A. Maurya, R. Kulkarni, A. Thamizhavel, D. Paudyal, and S. K. Dhar, *J. Phys. Soc. Jpn.* **85**, 034720 (2016).
- [48] R. E. Baumbach, H. Chudo, H. Yasuoka, F. Ronning, E. D. Bauer, and J. D. Thompson, *Phys. Rev. B* **85**, 094422 (2012).
- [49] Y. Matsumoto, M. Sugi, K. Aoki, Y. Shimizu, N. Kimura, T. Komatsubara, H. Aoki, M. Kimata, T. Terashima, and S. Uji, *J. Phys. Soc. Jpn.* **80**, 074715 (2011).
- [50] H. Aoki, N. Kimura, and T. Terashima, *J. Phys. Soc. Jpn.* **83**, 072001 (2014).
- [51] S. Süllow, M. C. Aronson, B. D. Rainford, and P. Haen, *Phys. Rev. Lett.* **82**, 2963 (1999).
- [52] H. Aoki, S. Uji, A. K. Albessard, and Y. Ōnuki, *Phys. Rev. Lett.* **71**, 2110 (1993).
- [53] H. Wilhelm and D. Jaccard, *Solid State Commun.* **106**, 239 (1998).
- [54] P. Haen, H. Bioud, and T. Fukuhara, *Phys. B (Amsterdam, Neth.)* **259–261**, 85 (1999).
- [55] D. Aoki, T. Combier, V. Taufour, T. D. Matsuda, G. Knebel, H. Kotegawa, and J. Flouquet, *J. Phys. Soc. Jpn.* **80**, 094711 (2011).
- [56] N. Kimura, N. Kabeya, H. Aoki, K. Ohyama, M. Maeda, H. Fujii, M. Kogure, T. Asai, T. Komatsubara, T. Yamamura, and I. Satoh, *Phys. Rev. B* **92**, 035106 (2015).
- [57] V. Taufour, U. S. Kaluarachchi, S. L. Bud'ko, and P. C. Canfield, *Phys. B (Amsterdam, Neth.)* (2017), doi:10.1016/j.physb.2017.08.065.
- [58] N. Kimura, M. Endo, T. Isshiki, S. Minagawa, A. Ochiai, H. Aoki, T. Terashima, S. Uji, T. Matsumoto, and G. G. Lonzarich, *Phys. Rev. Lett.* **92**, 197002 (2004).
- [59] M. Uhlarz, C. Pfleiderer, and S. M. Hayden, *Phys. Rev. Lett.* **93**, 256404 (2004).
- [60] T. R. Kirkpatrick and D. Belitz, *Phys. Rev. Lett.* **115**, 020402 (2015).
- [61] V. Taufour, U. S. Kaluarachchi, and V. G. Kogan, *Phys. Rev. B* **94**, 060410 (2016).
- [62] S. Nakamura, T. Sakakibara, Y. Shimizu, S. Kittaka, Y. Kono, Y. Haga, J. Pospíšil, and E. Yamamoto, *Phys. Rev. B* **96**, 094411 (2017).
- [63] S. Friedemann, W. J. Duncan, M. Hirschberger, T. W. Bauer, R. Kuchler, A. Neubauer, M. Brando, C. Pfleiderer, and F. M. Grosche, *Nat. Phys.* **14**, 62 (2017).